GEM TN-92-67

Jet-Energy Measurements with a Noncompensating Calorimeter System

H.P. Paar - University of California-San Diego,
R. Wigmans - Texas Tech University

February 20, 1992

Abstract:

We study how to obtain a measurement of a jet's energy with a calorimeter that consists of a noncompensating electromagnetic and a compensating or noncompensating hadronic section. We present results obtained with a simple algorithm that gets a best estimate of the true jet energy from the measured signals in each of the two calorimeter sections. The algorithm takes account of the event-to-event fluctuations in the energy deposits in the two calorimeter sections. If the hadronic calorimeter is compensating, all input data required for the method can be measured in beamtests of prototype calorimeter modules, using single electron and pion beams, and multiparticle beams (obtained from a target in a single pion beam). If the hadron calorimeter is noncompensating, additional knowledge is required regarding the jet fragmentation function and the electromagnetic energy fraction in hadronic shower development at SSC/LHC energies. The method works best for high jet energies (e.g. beyond 100 GeV) and its applicability can be extended to lower energies if the electromagnetic calorimeter is made thinner (in terms of nuclear interaction lengths). However, the noncompensating nature of the calorimeter system as a whole introduces nonlinearities in the signals, which cause a systematic uncertainty in the jet energy at the level of at least a few percent. Also, measurements of the (missing) transverse energy in SSC events are unlikely to benefit at all from this weighting procedure.

1. Introduction.

It is well known that one cannot have both the best electromagnetic resolution and compensation with one an the same calorimeter[1] . Compensation requires a sampling calorimeter, which unavoidably leads to a reduced electromagnetic energy resolution. The GEM and EAGLE collaborations are considering to have a noncompensating electromagnetic (EM) section in conjunction with a hadronic (HAD) section in order to optimize the electromagnetic resolution. We have studied to what extend jet energy measurements are compromised by this choice.

Although occasionally results have been presented on the so-called 'effective compensation' or 'weighting' or 'offline compensation' method, we remained sceptical for several reasons. The developers of this method published clear and concise papers[2,3,4] on the method as applied to single incident pions but not for jets (even though the H1-collaboration's single pion paper on weighting[3] contains a reference (their Ref. 5) to a jet paper 'in preparation'). The $L3$ collaboration reportedly[5] obtained effective compensation with two noncompensating calorimeters (BGO and Uranium/Gas) but the procedure was demonstrated experimentally only for jets from Z^0 decays at rest at LEP. In particular, none of the advocated methods was ever demonstrated to lead to improvements in the multiparticle energy resolution, although extensive experimental data of this type was available from prototype measurements.

Another reason for our scepticism concerns the fact that thus far the methods advocated for jets depend on Monte Carlos for jet fragmentation and hadronic shower development. In contrast with EGS which depends upon QED, the hadronic shower development Monte Carlos contain many assumptions and best guesses regarding the strong interaction cross sections as QCD is of little practical use here. We cannot judge to what extent the validity of the results depends upon having correct models for jet fragmentation and hadronic shower development. This is not tested in these Monte Carlo studies because the "data" are generated and then "analysed" with exactly the same physics assumptions. Thus by definition the physics of jet fragmention and hadronic shower development are known exactly, a situation very different from the one GEM will encounter[6] at the SSC. It seems undesirable to have possible discoveries involving high jet E_T, such as quark substructure, depend upon theoretical input of which the validity at SSC energies is impossible to ascertain experimentally.

We have found that a good estimate of the jet energy can be obtained with a simple algorithm that, on an event-by-event basis, uses the measured signals in the electromagnetic and hadronic calorimeter sections. The method does not rely upon detailed theoretical inputs but rather depends upon having a compensating hadronic section and upon having testbeam measurements on a prototype calorimeter with single electrons, single pions, and multiparticles. The latter can be obtained by placing a

target in the testbeam upstream of the calorimeter and requiring pions to interact in this target. It goes without saying that the known testbeam energy is not to be an input to the algorithm. Also we do not assume that the multiparticle topologies have any resemblance to the jet topologies in terms of multiplicity, particle species, momentum spectrum, or angle.

As indicated earlier we do not want to rely upon any particular model or 'black box' computer program. We have therefore done a computerised back of the envelope calculation. The computer program consists of a few hundred lines of FORTRAN code that are easy to understand[7] and calls to random number generators and integration routines. Execution time is an hour VAX780 equivalent for a run of 5 jet energies and 100 jets per energy point.

In this preliminary report we consider three different configurations:

1. EM and HAD sections with $e/h = 1.00$ each,
2. EM section with $e/h = 1.6$ and HAD section with $e/h = 1.3$,
3. EM section with $e/h = 2.0$ and HAD section with $e/h = 1.00$.

The e/h value describes the *energy independent* ratio of the calorimeter response (i.e. signal per unit energy) to electromagnetic (e.m.) and non-e.m. energy deposits[8] . Apart from the e/h value, each calorimeter section is also characterized by a value for e/mip, which relates the e.m. shower response to the response for minimum ionizing particles.

The first case is a calorimeter with compensating EM and HAD sections, the second case is chosen to describe a Liquid Argon detector with short shaping times, the third case simulates a BaF_2 EM section and a compensating HAD section. The contributions to the energy resolution from the sampling fluctuations and other instrumental effects have been omitted in the simulations, so as to isolate the features that have to do with the (non-)compensation.

2. Method.

2.1 Introduction.

The back of the envelope calculation consists of generating jets at a variety of energies (10, 20, 100, 500, 5000 GeV). Each particle in the jet is allowed to start its own shower in the calorimeter sections with shower development fluctuations included. The energy deposits, separated in e.m. and non-e.m. parts, are then used to calculate the calorimeter signals using the known responses of each section. Care is taken to treat the low energy non-showering charged hadrons (a few GeV and lower) in a reasonable way.

2.2 Jet-Fragmentation Function.

We used a simple fragmentation function similar to the one Dan Green used[9] in his studies. All particles are assumed to be pions and the fragmentation function is given by:

$$D(z) = (\alpha + 1)(1 - z)^{\alpha}/z \tag{2.1}$$

where α is a constant and $z_0 < z < 1$ with $z_0 = m_\pi/E_{\text{jet}}$. This leads to the usual logarithmic increase of the average particle multiplicity with jet energy. Each pion's charge is chosen at random but such that the average probability for π^0's is 0.4 and the average probabilities for a π^+ and a π^- are 0.3 each.

We find that (2.1) describes the LEP1 multiplicities reasonably well for $\alpha = 3$ while the higher energy CDF data favor $\alpha = 6$. Both values of α are therefore used as well as fragmentation into a single charged pion [$D(z) = \delta(1 - z)$ with δ the Dirac δ-function]. The resulting variation in the generated multiplicity allows a check on the model dependence of our conclusions.

2.3 Longitudinal Shower Development.

The π^0's and η's of the jet deposit all their energy in the EM section of the calorimeter. In the spirit of the back-of-the-envelope calculation, we use the parameterization of Bock *et al.*[10] for the shower development induced by the charged pions of the jet. This parameterization has two terms. One term corresponds to π^0 and η induced electromagnetic energy deposit (the e.m. shower component) and the other term corresponds to non-e.m. energy deposit. The parameterization includes a weight W that can be used to adjust these two terms relative to one another. We have used Don Groom's ansatz

for the average e.m.-fraction in a hadronic shower induced by a charged pion of energy E:

$$f_{\rm em} = 1 - \left(\frac{1}{E}\right)^{0.15} \tag{2.2}$$

to specify W as function of E. Eq. (2.2) agrees with Wigmans' anzatz[11] up to 1000 GeV and has been confirmed experimentally[12] by SPACAL.

The thickness of the calorimeter was assumed to be 10 nuclear interaction lengths ($L_{\rm int}$) for the hadronic section and 30 radiation lengths of material in the EM section.

2.4 Shower Development Fluctuations.

The starting point of each hadronic shower is taken from an exponential with a slope $1.5 \times L_{\rm int}$, where the factor 1.5 accounts for the fact that the pion interaction length is 1.5 times the particle data book value of $L_{\rm int}$ for protons. A delicate point concerns the change of material properties on the boundary between the EM and the HAD sections. After the starting point is chosen, the shower profile is integrated up to the boundary using the radiation length and the nuclear interaction length of the EM section. The leftover energy $E_{\rm left}$ is then used to calculate, using now the radiation length and the nuclear interaction length of the HAD section, from what value $z = z_1$ the integrated energy deposit between z_1 and infinity equals $E_{\rm left}$. Using this value of z_1, the true deposited energy is calculated by integrating from z_1 to the end of the HAD section. We call the deposited energies $E_{\rm 1dep}$ and $E_{\rm 2dep}$ respectively for the EM and HAD sections. With Bock's parameterization we know the e.m. and non-e.m. components of $E_{\rm 1dep}$ and of $E_{\rm 2dep}$.

The e.m. component in the hadronic shower development is fluctuated according to experimental results obtained[12] by SPACAL. We used

$$\frac{\sigma(f_{\rm em})}{f_{\rm em}} = 0.435 - 0.052 \ln E \tag{2.3}$$

This formula has been obtained for pions in the energy range 5-150 GeV, we use it at higher energies as well. Our results turn out to be very insensitive to the particular form of (2.3).

2.5 CALORIMETER SIGNALS.

In order to calculate the calorimeter signals, we normalize on the response to non-e.m. shower energy deposits (the h component). Electromagnetic energy deposits are thus multiplied by the e/h value of the calorimeter section in which they occur* As an example, we consider a 100 GeV charged pion showering in configuration 2 (see sect. 1). Let us assume that 50 GeV is deposited in e.m. form, 40 GeV in the EM calorimeter section and 10 GeV in the HAD one. The remaining 50 GeV is deposited in non-e.m. form, 5 GeV in the EM section and 45 GeV in the HAD section. The total calorimeter signal is then calculated as $40 \times 1.6 + 5 \times 1.0 + 10 \times 1.3 + 45 \times 1.0 \;=\; 127$ GeV. Low energy charged pions will not shower but instead range out as muons would. The energy lost by these particles is thus weighted with a factor mip/h [$= (e/h)/(e/mip)$] in order to obtain the calorimeter signal.

Summing over jet fragments we obtain the detected energies (the calorimeter signals) $E_{1\mathrm{det}}$ and $E_{2\mathrm{det}}$ for the EM and HAD sections, respectively.

3. Results.

3.1 OVERVIEW.

We first give an overview of results and take as an example the case of a BaF_2 EM section and a compensating HAD section, case 3 of Sec. 1, and a jet energy of 500 GeV. In Fig. 1 we show the multiplicity distribution, charged and neutral pions both included. The value for α in (2.1) was taken to be $\alpha = 3$. In Fig. 2 we show the distributions of the energies $E_{1\mathrm{dep}}$ and $E_{2\mathrm{dep}}$, deposited in the EM and HAD sections respectively. The deposited energy in section 1 is quite large due to the fact that on average 40% of the jet's energy is assumed to be in π^0's. Furthermore a lot of electromagnetic energy is deposited early in the charged pion induced hadronic shower by π^0's and η's. produced in the hadronic shower development. It is clear that the EM section plays a crucial role in the measurement of the jet's energy. In Fig. 3 we show the detected energies $E_{1\mathrm{det}}$ and $E_{2\mathrm{det}}$ in the EM and HAD sections respectively. The effects of the assumed (e/h)-ratio's (2.0 and 1.0 respectively) are clearly visible when one compares Figs. 2 and 3.

In Fig. 4 we show a scatterplot of $E_{1\mathrm{det}}$ (ordinate) against E_{det} (abscissa) and the projection E_{det}. Several things should be noted in Fig. 4:

- The relative width of the detected jet energy is quite large: $\sigma(E_{\mathrm{det}})/E_{\mathrm{det}} = 11\%$ at $E_{\mathrm{jet}} = 500\,\mathrm{GeV}$.

* Please note that we distinguish between the observable energy dependent e/π signal ratio and the energy independent e/h value.

- The points in the scatterplot lay in a narrow band indicating a tight correlation between $E_{1\mathrm{det}}$, $E_{2\mathrm{det}}$, and E_{det}.
- The band is approximately a straight line that extrapolates to the points $(E_{\mathrm{det}}, E_{1\mathrm{det}}) = (1000\,\mathrm{GeV}, 1000\,\mathrm{GeV})$ and $(500\,\mathrm{GeV}, 0\,\mathrm{GeV})$.

These values for the intercepts are understood as follows. In the extreme case of a jet fragmenting entirely into π^0's, all its energy will be deposited in the EM section, thus $E_{2\mathrm{dep}} = E_{2\mathrm{det}} = 0$ and $E_{\mathrm{det}} = E_{1\mathrm{det}}$. Because $e/h = 2.00$ for the EM section, $E_{1\mathrm{det}} = 2.00 \times E_{1\mathrm{dep}} = 2.00 \times E_{\mathrm{jet}}$. This gives the intercept at $(1000\,\mathrm{GeV}, 1000\,\mathrm{GeV})$ for the present example with $E_{\mathrm{jet}} = 500\,\mathrm{GeV}$. In the other extreme case all the jet energy is deposited in the HAD section, thus $E_{1\mathrm{dep}} = E_{1\mathrm{det}} = 0$. As the HAD section is compensating we have $E_{\mathrm{det}} = E_{2\mathrm{det}} = E_{\mathrm{jet}}$. This gives the other intercept at $(500\,\mathrm{GeV}, 0\,\mathrm{GeV})$. Note how we calculate the position of the line in the scatterplot using only the (e/h)-ratio of the EM (and, trivially, of the HAD) section.

Conversely, the slope of the line should be independent of the jet energy as it is entirely determined by the (e/h)-ratio of the EM section. This is confirmed in Fig. 5 where the same scatterplot is given for jet energies of 20, 100, 500, and 5000 GeV. It is seen that the correlation between the signals in the two calorimeter sections deteriorates at decreasing energy. At the higher energies the lines all have the same slope within a few percent and have intercepts in accordance with the simple argument given above.

The spread of the points along the lines in the various scatterplots is caused by the fluctuations in the jet's multiplicity, the fluctuations in the jet's π^0 fraction, and the fluctuations in the shower development (in starting point and in e.m. shower fraction). Given the fact that the lines in the scatterplots for jet energies of 100 GeV and greater are essentially straight with a well defined energy-independent slope and with calculable intercepts with the axes, we expect that different fragmentation functions and different e.m. fractions in the hadronic shower development would position points differently along one and the same line. That this is indeed the case is shown Fig. 6 and 7 for a jet fragmentation function (2.1) with $\alpha = 6$ and for jets consisting of a single charged pion respectively. It is seen that the points in the scatterplots are laying along one and the same essentially straight line to within a few percent for jet energies of 100 GeV and larger. The cluster of points along the horizontal axis in Fig. 7 is due to leakage out the back of the HAD section (only seen for single pions).

The few percent deviations, mentioned twice above, are important for the signal linearity of the calorimeter. We come back to this point in Sec. 3.3.

These results lead to an important conjecture: We can measure the position of the line in the scatterplot by measuring the multiparticle response of a prototype in a testbeam without worrying about whether the multiparticle topology is sufficiently similar to the jet topology. The intercepts of the extrapolated line with the axes give the (e/h)-ratio of the EM and HAD section respectively.

The conjecture can be checked by doing testbeam measurements with single pions and multiparticles derived from interactions in a target just upstream of the calorimeter and varying the testbeam energy. For a fixed testbeam energy the points should be distributed differently along one and the same straight line (with the same intercepts with the axes). Varying the testbeam energy from say 100 GeV to 2 TeV should then lead to a family of lines in a $E_{1\mathrm{det}}$ versus E_{det} scatterplot, each with a slope and a location consistent with the other lines. The SSC injector will have a 2 TeV proton testbeam to do this with and given the simple model-independent calculation of the intercepts, one can extrapolate the calorimeter response with some confidence from 2 TeV to the highest SSC energies. [Of course many other instrumental effects must be checked separately but that is outside the scope of this memo.]

This conclusion holds only for calorimeters with a compensating HAD section. If the HAD section is noncompensating, one also needs to know $< f_{\mathrm{em}} >$, where the average is over the a-priori unknown jet fragmentation function at the appropriate jet energy, as will be shown in section 3.5.

3.2 Jet-Energy Estimation.

As can be seen from the scatterplots in Figs. 5, 6, and 7 and also from the reasoning that lead to the calculation of the intercepts, each jet energy has a corresponding well-defined line in the scatterplot and all lines have the same slope. For a fixed jet energy, fluctuations in the jet's multiplicity, fluctuations in the jet's e.m. fraction, and fluctuations in the charged hadronic shower development (in starting point and in e.m. shower fraction) merely distribute points along the corresponding well-defined line in the $E_{1\mathrm{det}}$ versus E_{det} scatterplot. In other words: given $E_{1\mathrm{det}}$ and $E_{2\mathrm{det}}$, we can find a coordinate in the scatterplot, draw the line with the slope from the test beam measurements through it, find the intercept with the horizontal axis where $E_{1\mathrm{det}} = 0$, and find the jet energy. We call the so obtained jet energy E_{cor}. From the reasoning given above, it is given by

$$E_{\mathrm{cor}} = \frac{E_{1\mathrm{det}}}{(e/h)} + E_{2\mathrm{det}} \tag{3.1}$$

where (e/h) is the (e/h)-ratio of the EM section: $(e/h)_{\mathrm{EM}}$. Using this procedure we plot the corrected jet energies for 20, 100, 500, and 5000 GeV jet energies in Fig. 8 for the jet fragmentation (2.1) with $\alpha = 3$. It is seen that the resolutions are greatly improved for jet energies of 100 GeV and greater. Inspection of (3.1) immediately explaines why the method works best at large and poorly at low jet energies: one could write down this equation from first principles except that one would need an extra term concerning the non-e.m. energy deposit in the EM section. This term is neglected in (3.1) and this

approximation is better fulfilled the higher the jet energy. The approximation is also better fulfilled the thinner the EM section is in terms of nuclear interaction lengths. As the number of radiation lengths in the EM section is fixed by the requirement of electromagnetic shower containment, the "hadronic thin-ness" condition points to the use of a high Z absorber material in the EM section: uranium would be better (by a factor 2) than BaF_2. In the case of a uranium EM section, the method would therefore work better and down to lower energies.

3.3 LINEARITY.

We have studied the linearity of the corrected jet energy by comparing $E_{\rm cor}$ and $E_{\rm jet}$, again for the BaF_2 calorimeter configuration (case 3, sect. 1). The results are given in Fig. 9 for the usual three different jet fragmentation cases: (2.1) with $\alpha = 3$ and 6, and single charged pions. The responses have been normalized at 10 GeV. There are clearly unacceptably large 10% non-linearities between 5 and 5000 GeV and these non-linearities have a $\pm 2\%$ dependence upon the jet fragmentation function. These nonlinearities are clearly due to the noncompensation of the calorimeter system as a whole. Looking at (3.1), we see that non-e.m. energy deposited in the EM calorimeter section is weighted by a factor 1/2, which should not be done if one knew of a method to avoid it. This reduces the total signal by a larger fraction at low energy than at high energy, since at high energy most of the non-e.m. component is deposited in the HAD section. In other words, the same mechanism that makes the improvement in the energy resolution energy dependent causes the signal nonlinearities. Figure 9 shows that these nonlinearities do make the estimate of the true jet energy somewhat dependent on the jet fragmentation function.

All is not lost however because we can plan on beam tests with a 2 TeV proton testbeam at the SSC. From this point on towards higher energies, the effects are small. In addition, a global correction might be made that is some average over a family of curves as in Fig. 9, and that accounts for the effects of the nonlinearities when calculating the jet energy. These nonlinearities are nevertheless worrysome and need more detailed studies.

3.4 Resolution.

The effects of noncompensation on the hadronic energy resolutions obtained with the BaF_2 calorimeter configuration after weighting are summarized in Fig. 10, for jets with $\alpha = 3$. Similar results are obtained for fragmentation with $\alpha = 6$ and for single charged pions. Also shown is the resolution in the uncorrected jet energy for jets with $\alpha = 3$. It is seen that the resolutions are greatly improved relative to the uncorrected case, especially for high jet energies. At 100 GeV, the uncertainty in the jet energy coming from the effects of noncompensation is seen to improve from 11% to about 4% due to the weighting algorithm. At higher energies the improvement is even larger.

The effect of different jet fragmentation functions is seen to be small because the cases shown in Fig. 10 correspond to an extreme variation in the jet fragmentation. However, it should be pointed out that one effect of the nonlinearities discussed in the previous subsection may be that the jet energies are systematically determined too high or too low by a few percent and that this effect may well be larger than the resolutions shown in fig. 10 for the TeV region.

At energies below 100 GeV, the improvement in the energy resolution achieved with this weighting algorithm becomes rapidly marginal. This can be understood from the fact that the condition that e.m. energy be deposited in the EM calorimeter section and non-e.m. energy in the HAD one in order to make the method work, is far from being met. As a consequence, the measurements of transverse energy and missing transverse energy are likely not to benefit from such a weighting procedure. The (missing) transverse energy of an SSC event involves frequently contributions from a multitude of jets of relatively low energy and, therefore, the (missing) E_T will not be measured more accurately than the typical jet contributing to it.

3.5 Noncompensating Hadronic Section.

In this subsection, we investigate in which respect the conclusions that we have drawn so far have to be changed if not only the EM section, but also the HAD section of the calorimeter system is noncompensating $[(e/h)_{\mathrm{HAD}} \neq 1]$, as in the LAr option of GEM. We generated jets at energies from 20 to 5000 GeV and let these develop showers in configuration 2 (see sect. 1) for this purpose.

In Fig. 11 the scatterplot of $E_{1\mathrm{det}}$ (ordinate) is shown against E_{det} (abscissa) for jets according to the jet-fragmentation function (2.1) with $\alpha = 3$. In comparing this scatterplot with the one from Fig. 5, the following things should be noted:

- The points in the scatterplot still lay along a narrow band indicating a tight correlation between $E_{1\mathrm{det}}$, $E_{2\mathrm{det}}$, and E_{det}.

– This band again extrapolates to the point $(E_{\rm det}, E_{\rm 1det}) = (1.6 \times E_{\rm jet}, 1.6 \times E_{\rm jet})$, but it turns out that the intercept with the horizontal axis cannot be calculated in a model independent way for this detector configuration.

If the HAD section is noncompensating, the calculation for the intercepts changes: the band in the scatterplot is not straight anymore and the intercept with the horizontal axis is shifted to higher $E_{\rm det}$ by an amount

$$\Delta = [(e/h)_{\rm HAD} - 1] < f_{\rm em} > E_{\rm jet} \tag{3.2}$$

where $< f_{\rm em} >$ is the energy dependent e.m. fraction $f_{\rm em}$ in hadronic showers, averaged over the a-priori unknown fragmentation function $D(z)$ at the given jet energy. Note that the shift $\Delta = 0$ if and only if $(e/h)_{\rm HAD} = 1.00$ and that for a calorimeter with a compensating hadronic section the condition $\Delta = 0$ is fulfilled independent of the value of $f_{\rm em}$ and thus independent of the value of $f_{\rm em}$ or its energy dependence as well as independent of the fragmentation function. This is shown schematically in Fig. 12. Note that in this case the intercept with the horizontal axis cannot be determined with a prototype in a testbeam since the multiparticle topology is not the same as the jet particle topology.

4. Discussion.

We have investigated to what extent the hadronic performance of a calorimeter system consisting of an EM and an HAD section is affected by the fact that either the EM section or both sections are noncompensating, and if and how weighting schemes could be employed to restore the performance. We have shown that such weighting schemes work only perfectly in the idealized situation in which all the e.m. jet energy is deposited in the EM calorimeter section and all the non-e.m. energy in the HAD section, which has to be compensating for that purpose. This idealized situation is better approximated at high energy than at low energy and, therefore, weighting schemes might be useful for improving the resolution of very high-energy jets.

An important point about calorimeter signals is whether linearity, lineshape, and resolution are knowable for jets at SSC/LHC energies. It is not important which choice of techniques gives the best resolution on paper if that choice requires detailed theoretical knowledge of for example jet fragmentation and hadronic shower development at SSC energies. By knowable we mean that *all* required input information for the calculation of the corrected jet energy must be measurable with prototypes in testbeams without theoretical inputs.

We have shown that jet energies of 100 GeV and higher can be measured reasonably precisely using a simple algorithm for a calorimeter consisting of a combination of a highly noncompensating BaF_2 EM section combined with a compensating HAD section. *All* required input data can be obtained in testbeams with prototypes. The method will work down to lower energies if the EM section is made of higher-Z material.

We have also shown that the use of a noncompensating HAD section requires additional theoretical inputs regarding the jet fragmentation function at SSC energies and the e.m. fraction and its energy dependence in charged hadron induced showers. Therefore, we conclude that it is desirable to have a calorimeter system with a compensating HAD section, even if the EM section is (strongly) noncompensating.

The fact that always some fraction of the non-e.m. jet energy will be deposited in the EM calorimeter section and the fact that this fraction on average increases at decreasing energy limits the applicability of weighting schemes. We have shown that quite severe signal nonlinearities are introduced, which moreover do depend on details of the jet fragmentation function, even if the HAD section is compensating. Apart from that, weighting schemes are unlikely to be of any use at all for improving the resolution of (missing) transverse energy and of other quantities determined by the precision with which particles below 100 GeV are measured.

5. Acknowledgements.

We acknowledge enlightening discussions with Jim Branson and Mike Sivertz. Fabio Riccardi helped us making the figures.

REFERENCES

1. R. Wigmans, Performance and limitations of hadron calorimeters, preprint CERN-PPE/91-205 (1991).
2. H. Abramowicz *et al.* (CDHS collaboration), NIM **180** (1981) 429.
3. W. Braunschweig *et al.* (H1 collaboration), NIM **A265** (1988) 419.
4. W. Braunschweig *et al.* (H1 collaboration), NIM **A275** (1989) 246.
5. Y. Kamyshkov, priv. comm.
6. It would be interesting to let one physicist apply his favourite weighting procedure to jets that were generated by another physicist.
7. The code is available upon request. Transfer by E-mail is easiest, send request to 27833::HPAAR.
8. R. Wigmans, Ann. Rev. Nucl. Part. Sci. **41** (1991) 133, and references therein.
9. D. Green, Dijet Spectroscopy at High luminosity, Fermilab-Conf-90/151.
10. R.K. Bock, T. Hansl-Kozanecka, and T.P. Shah, NIM **186** (1981) 533.
11. R. Wigmans, NIM **A265** (1988) 273.
12. D. Acosta *et al.* (SPACAL collaboration), Lateral Shower profiles in a Scintillating Fiber Calorimeter, preprint CERN-PPE/91-223 (1991), to be published in NIM.

FIGURE CAPTIONS

1. The multiplicity distribution for pions in 500 GeV jets fragmented according to (2.1) with $\alpha = 3$.
2. The energy deposit $E_{1\mathrm{dep}}$ in the EM section and $E_{2\mathrm{dep}}$ in the HAD section for 500 GeV jets fragmented according to (2.1) with $\alpha = 3$.
3. The detected energy $E_{1\mathrm{det}}$ in the EM section and $E_{2\mathrm{det}}$ in the HAD section for 500 GeV jets fragmented according to (2.1) with $\alpha = 3$.
4. Scatterplot of $E_{1\mathrm{det}}$ (ordinate) against E_{det} (abscissa) and the projection E_{det} for 500 GeV jets fragmented according to (2.1) with $\alpha = 3$.
5. Scatterplot of $E_{1\mathrm{det}}$ (ordinate) against E_{det} (abscissa) for jets of 20, 100, 500 and 5000 GeV fragmented according to (2.1) with $\alpha = 3$.
6. Scatterplot of $E_{1\mathrm{det}}$ (ordinate) against E_{det} (abscissa) for jets of 20, 100, 500 and 5000 GeV fragmented according to (2.1) with $\alpha = 6$.
7. Scatterplot of $E_{1\mathrm{det}}$ (ordinate) against E_{det} (abscissa) for single charged pions of 20, 100, 500 and 5000 GeV.
8. Corrected jet energy distributions for 20, 100, 500, and 5000 GeV jets fragmented according to (2.1) with $\alpha = 3$.
9. The linearity of the corrected jet energy E_{cor} with the (true) jet energy E_{jet} for three different jet fragmentation cases, see text.
10. The resolution of the corrected jet energy E_{cor} for jets fragmented according to (2.1) with $\alpha = 3$ and for single pions. For comparison the resolution of the uncorrected jet-energy for jets ($\alpha = 3$) is shown too.
11. Scatterplot of $E_{1\mathrm{det}}$ (ordinate) against E_{det} (abscissa) for jets of 20, 100, 500 and 5000 GeV fragmented according to (2.1) with $\alpha = 3$ for a LAr calorimeter.
12. Schematic representation of the expected location of the points in the $E_{1\mathrm{det}}$ versus E_{det} scatterplot. The effect of a noncompensating hadronic section is a shift of the intercept with the horizontal axis with the indicated magnitude.

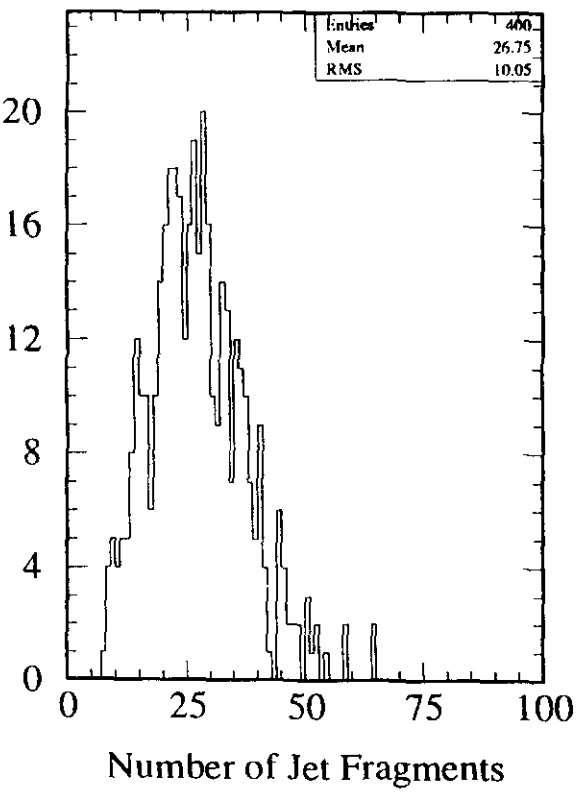
Entries 400
Mean 26.75
RMS 10.05
20
16
12
8
4
0
0
25
50
75
100
Number of Jet Fragments

Figure 1

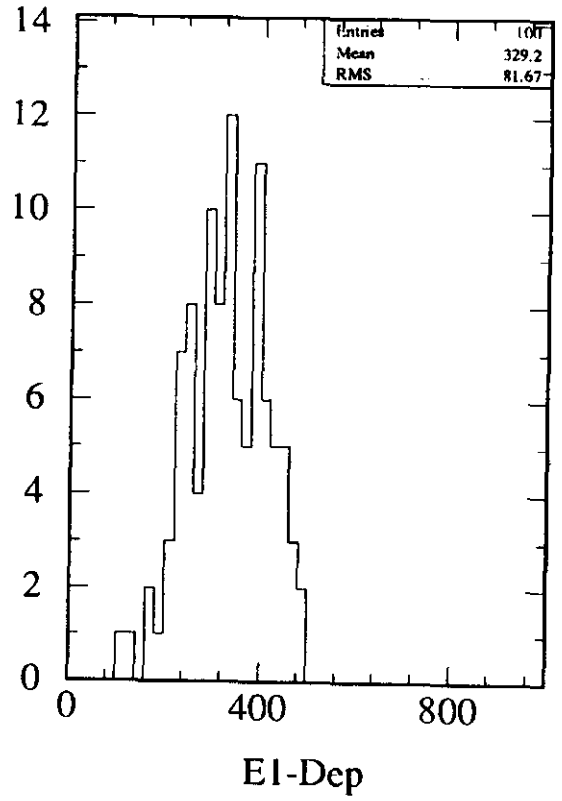
Entries 100
Mean 329.2
RMS 81.67
14
12
10
8
6
4
2
0
0
400
800
E1-Dep

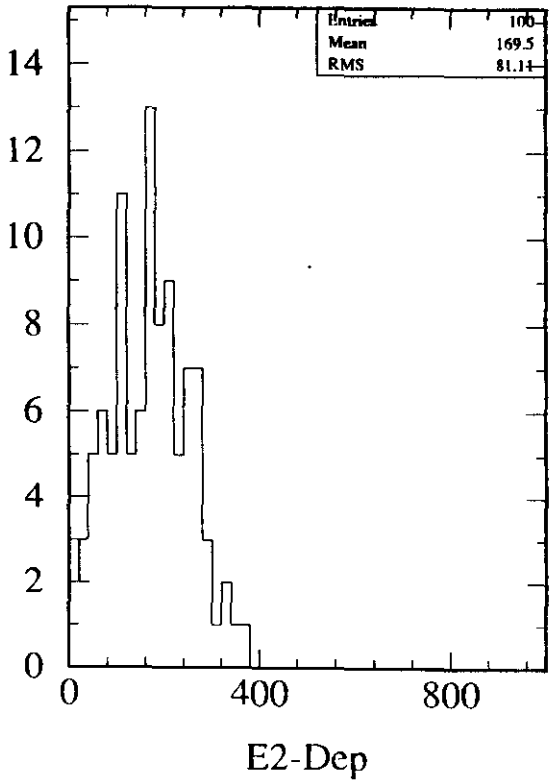
Entries 100
Mean 169.5
RMS 81.14
14
12
10
8
6
4
2
0
0
400
800
E2-Dep

Figure 2

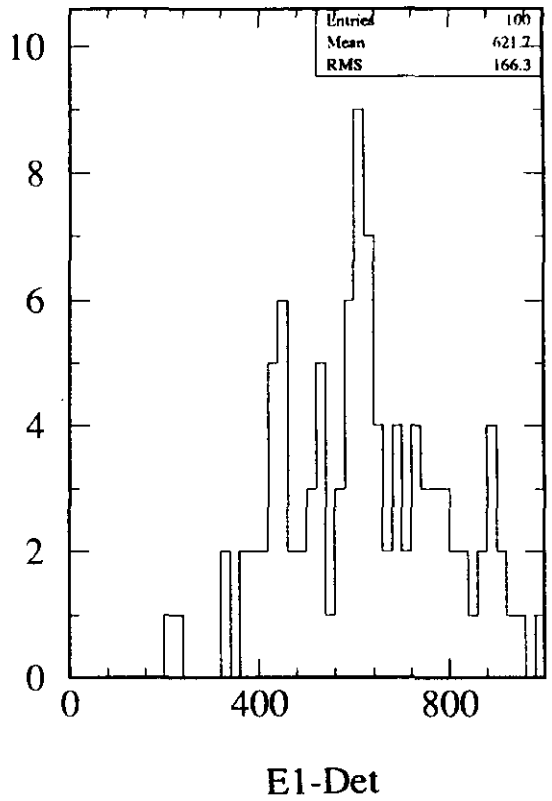
Entries 100
Mean 621.2
RMS 166.3
10
8
6
4
2
0
0
400
800
E1-Det

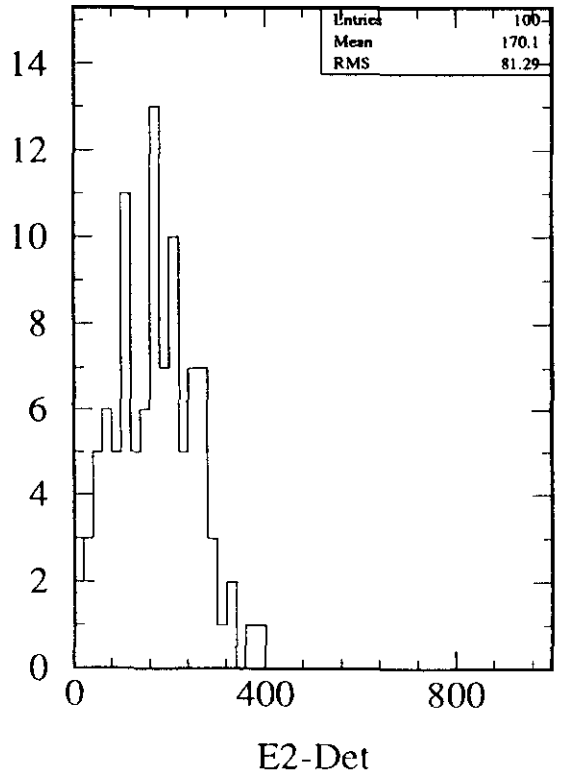
Entries 100
Mean 170.1
RMS 81.29
14
12
10
8
6
4
2
0
0
400
800
E2-Det

Figure 3

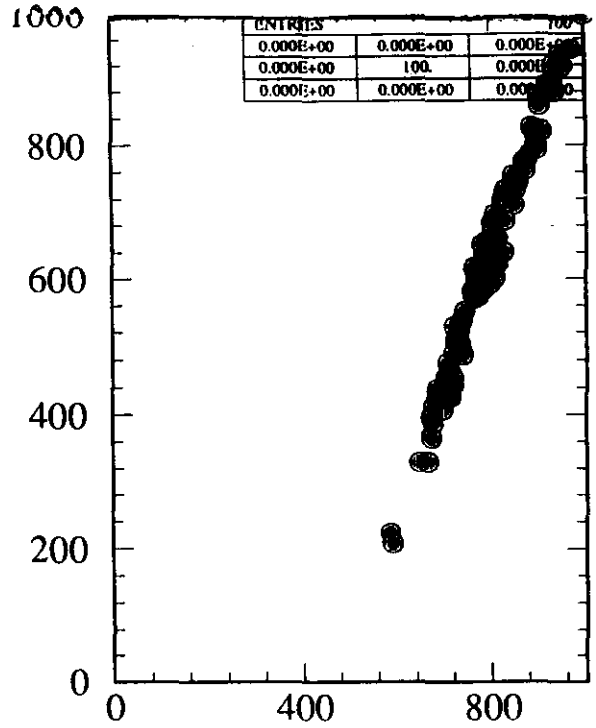

E1-Det vs E-Det

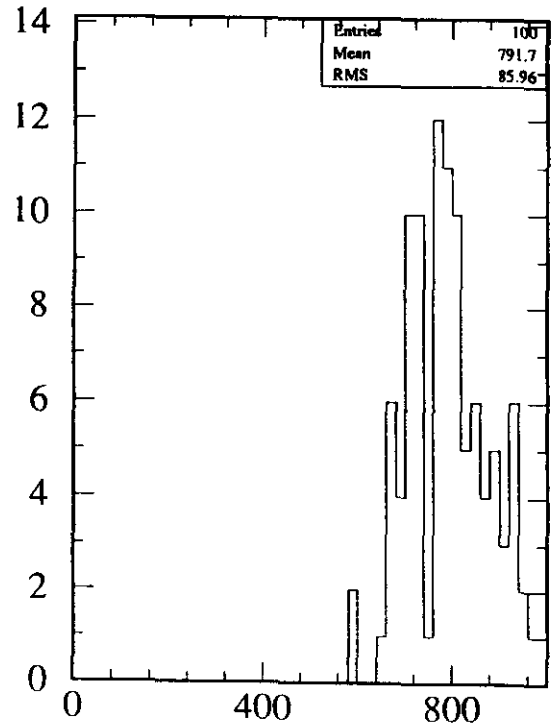

E-Det

Figure 4

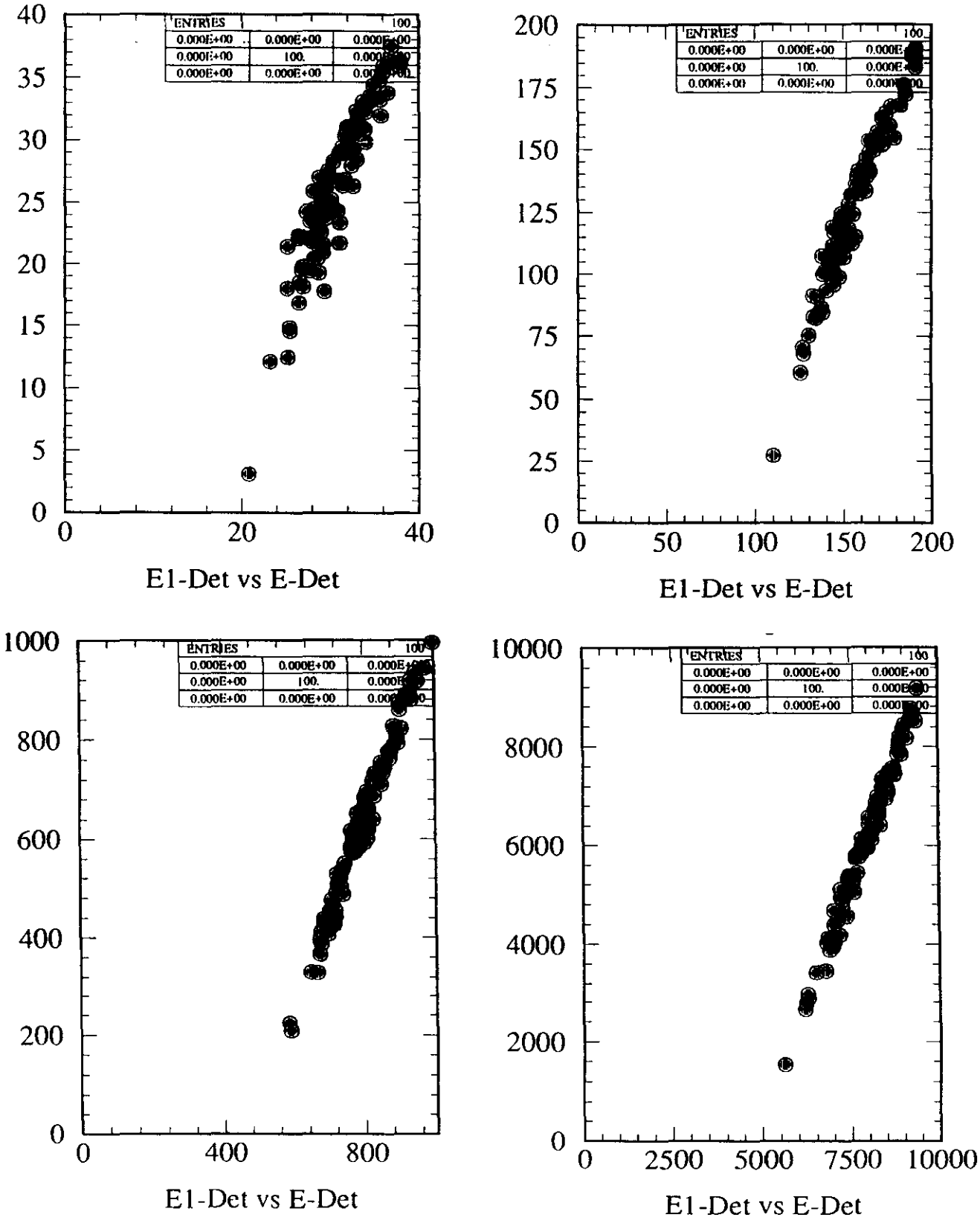
ENTRIES 100.
0.000E+00 0.000E+00 0.000E+00
0.000E+00 100. 0.000E+00
0.000E+00 0.000E+00 0.000E+00
E1-Det vs E-Det
E1-Det vs E-Det
E1-Det vs E-Det
E1-Det vs E-Det

Figure 5

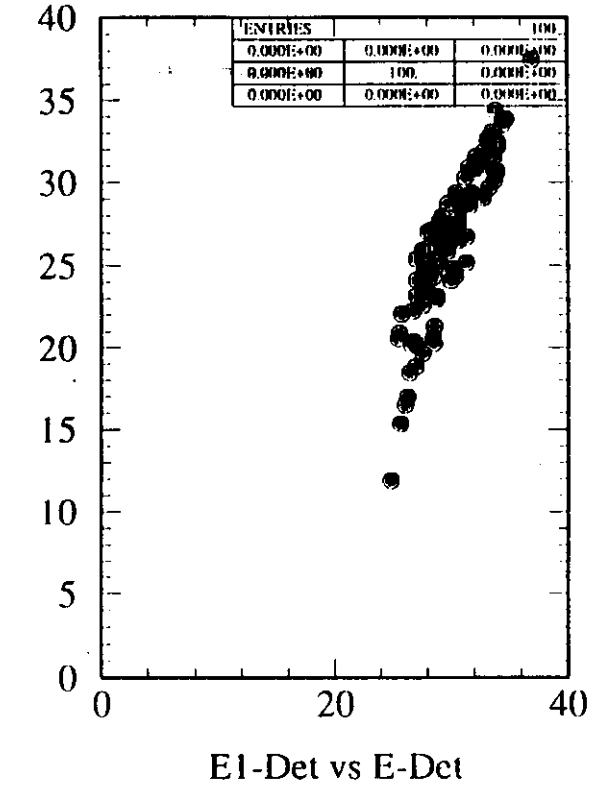
ENTRIES 100.
0.000E+00 0.000E+00 0.000E+00
0.000E+00 100. 0.000E+00
0.000E+00 0.000E+00 0.000E+00
E1-Det vs E-Det

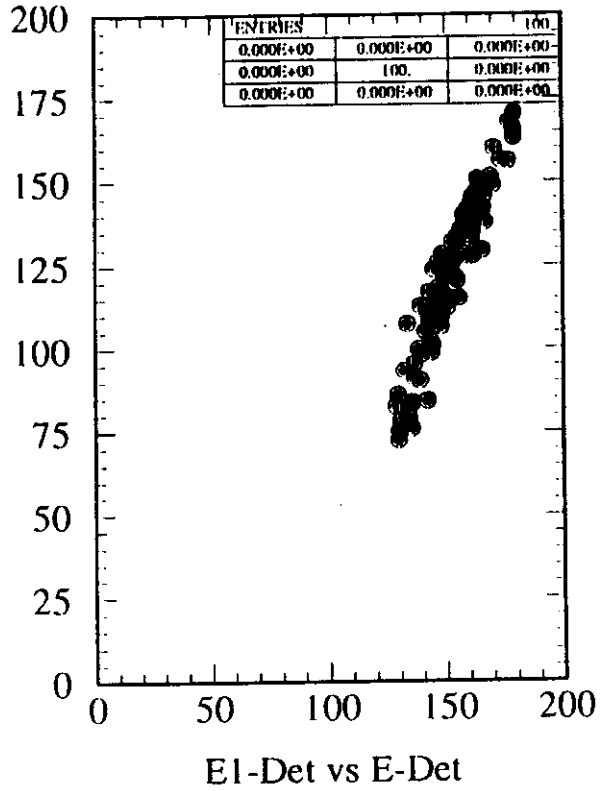
ENTRIES 100.
0.000E+00 0.000E+00 0.000E+00
0.000E+00 100. 0.000E+00
0.000E+00 0.000E+00 0.000E+00
E1-Det vs E-Det

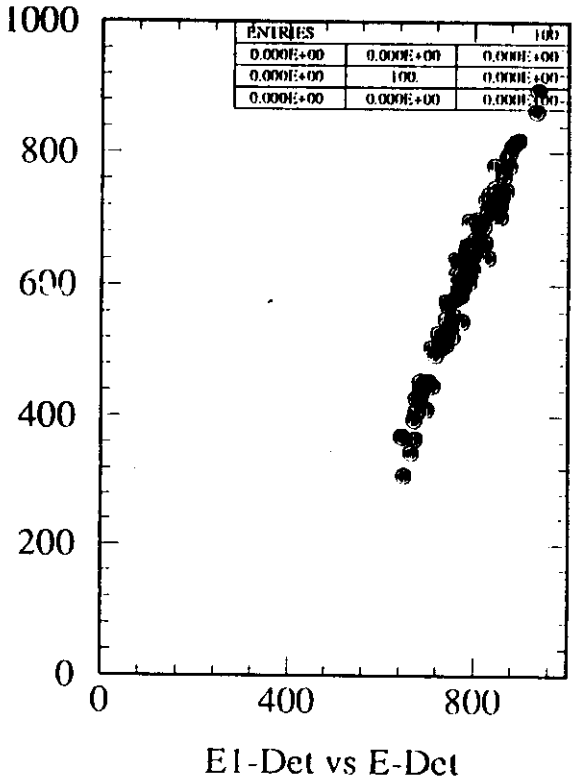
ENTRIES 100
0.000E+00 0.000E+00 0.000E+00
0.000E+00 100. 0.000E+00
0.000E+00 0.000E+00 0.000E+00
E1-Det vs E-Det

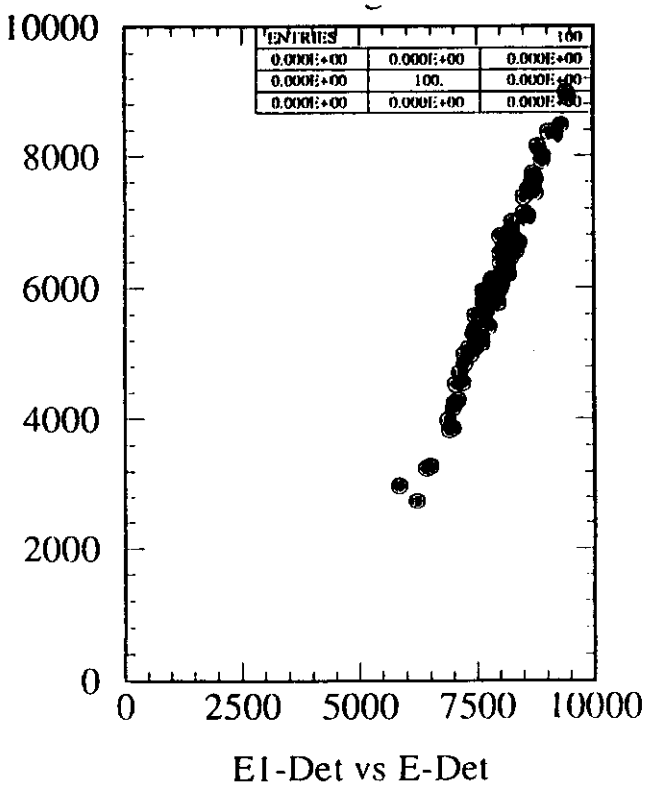
ENTRIES 100
0.000E+00 0.000E+00 0.000E+00
0.000E+00 100. 0.000E+00
0.000E+00 0.000E+00 0.000E+00
E1-Det vs E-Det

Figure 6

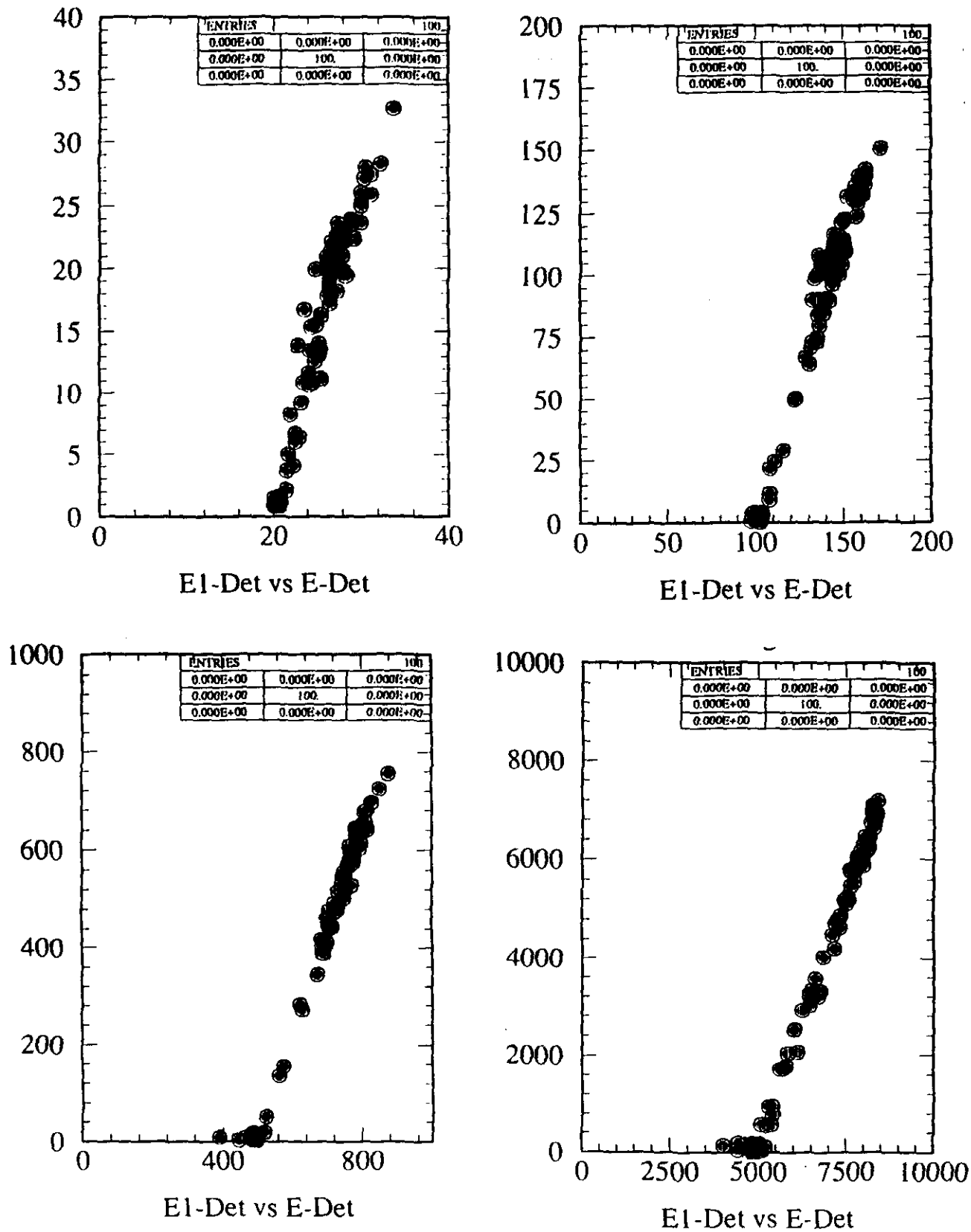
ENTRIES 100.
0.000E+00 0.000E+00 0.000E+00
0.000E+00 100. 0.000E+00
0.000E+00 0.000E+00 0.000E+00
E1-Det vs E-Det
E1-Det vs E-Det
E1-Det vs E-Det
E1-Det vs E-Det

Figure 7

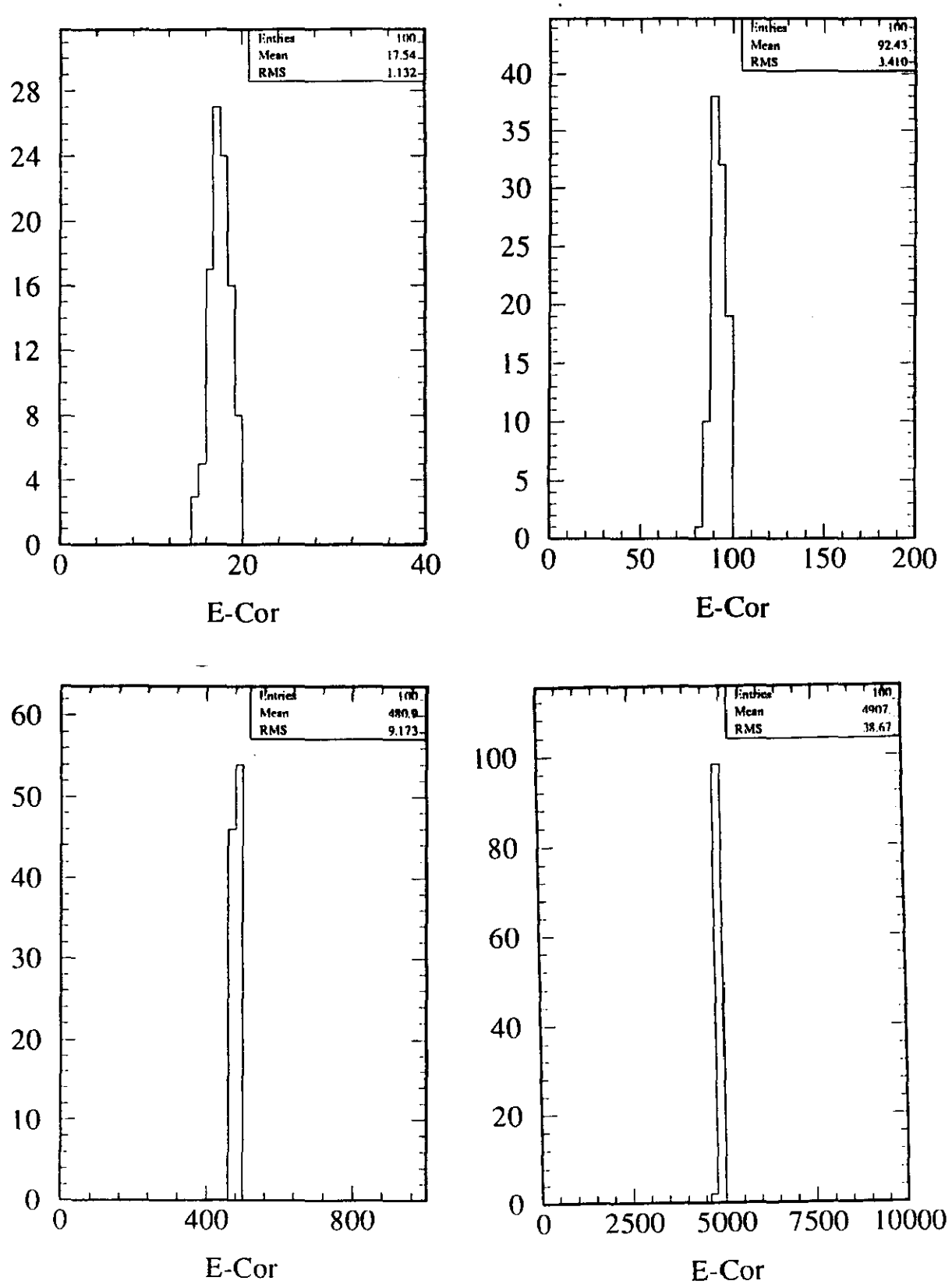
Entries 100
Mean 17.54
RMS 1.132
E-Cor
Entries 100
Mean 92.43
RMS 3.410
E-Cor
Entries 100
Mean 480.9
RMS 9.173
E-Cor
Entries 100
Mean 4907.
RMS 38.67
E-Cor

Figure 8

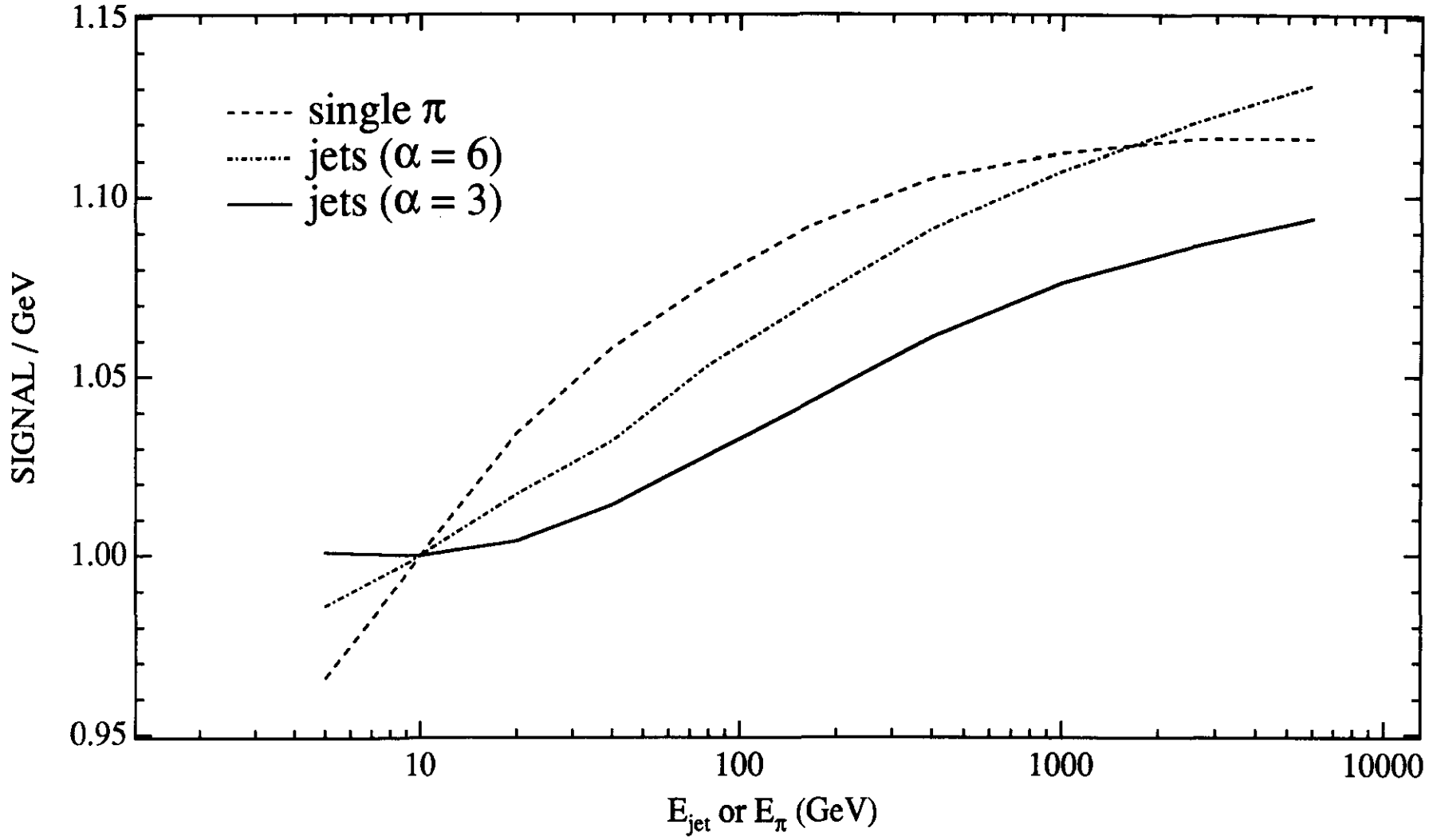
1.15
1.10
1.05
1.00
0.95
SIGNAL / GeV
single π
jets (α = 6)
jets (α = 3)
10
100
1000
10000
E_jet or E_π (GeV)

Figure 9

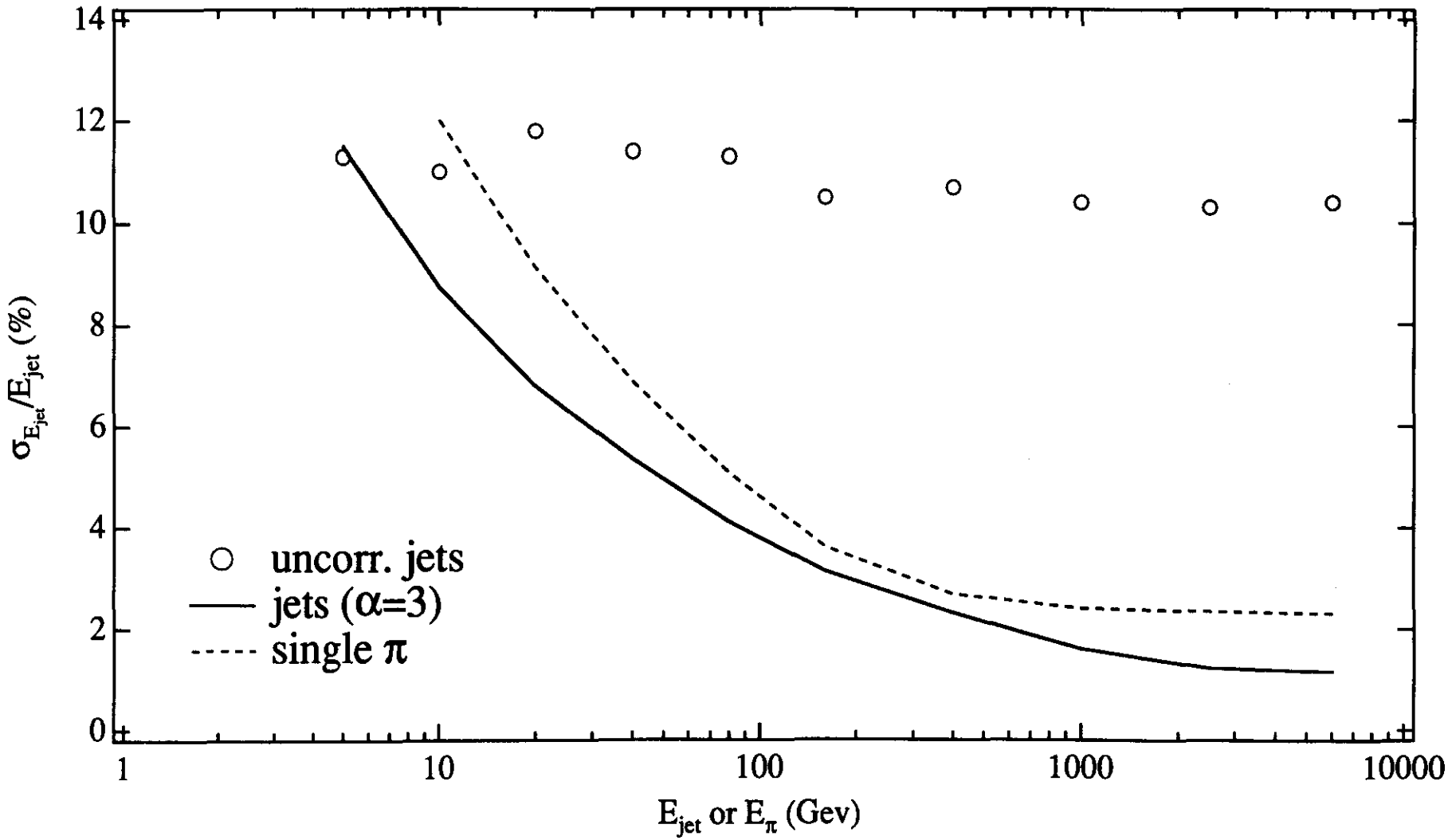
14
12
10
8
6
4
2
0
$\sigma_{E_{jet}}/E_{jet}$ (%)
uncorr. jets
jets (α=3)
single π
1
10
100
1000
10000
E_{jet} or E_{π} (Gev)

Figure 10

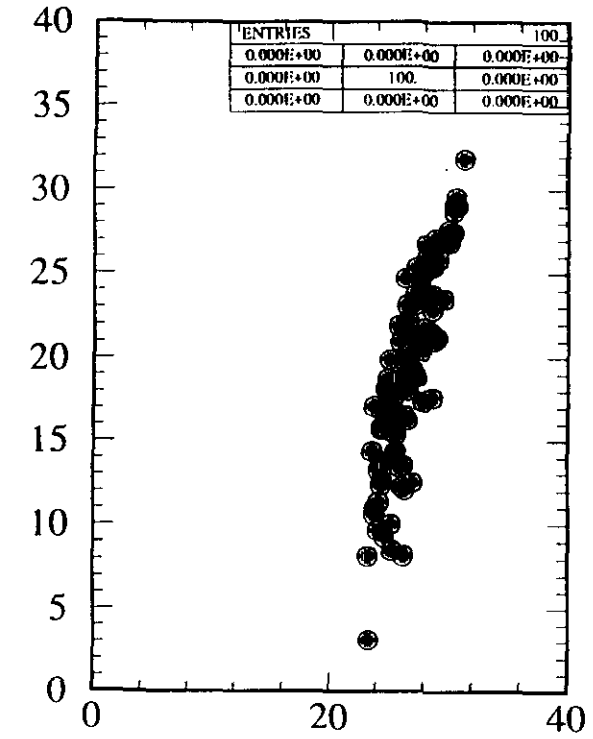
ENTRIES 100
0.000E+00 0.000E+00 0.000E+00
0.000E+00 100. 0.000E+00
0.000E+00 0.000E+00 0.000E+00
0 5 10 15 20 25 30 35 40
0 20 40
E1-Det vs E-Det

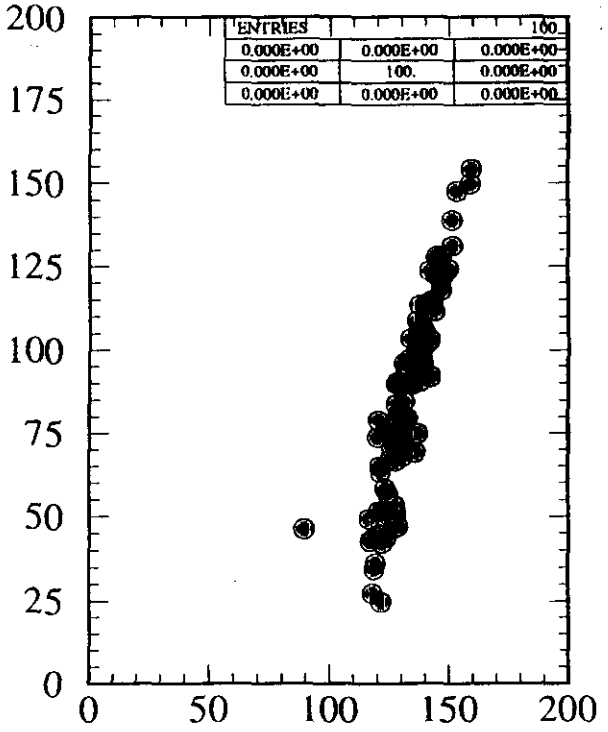
ENTRIES 100
0.000E+00 0.000E+00 0.000E+00
0.000E+00 100. 0.000E+00
0.000E+00 0.000E+00 0.000E+00
0 25 50 75 100 125 150 175 200
0 50 100 150 200
E1-Det vs E-Det

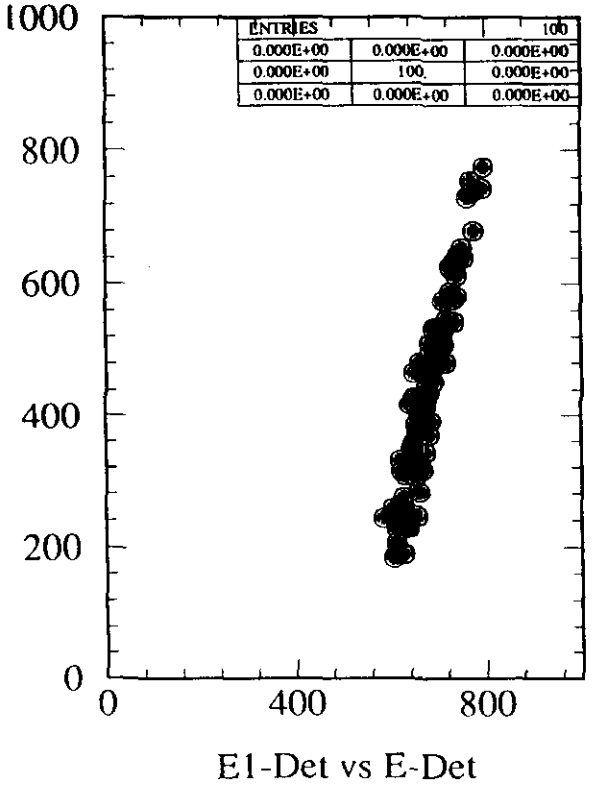
ENTRIES 100
0.000E+00 0.000E+00 0.000E+00
0.000E+00 100. 0.000E+00
0.000E+00 0.000E+00 0.000E+00
0 200 400 600 800 1000
0 400 800
E1-Det vs E-Det

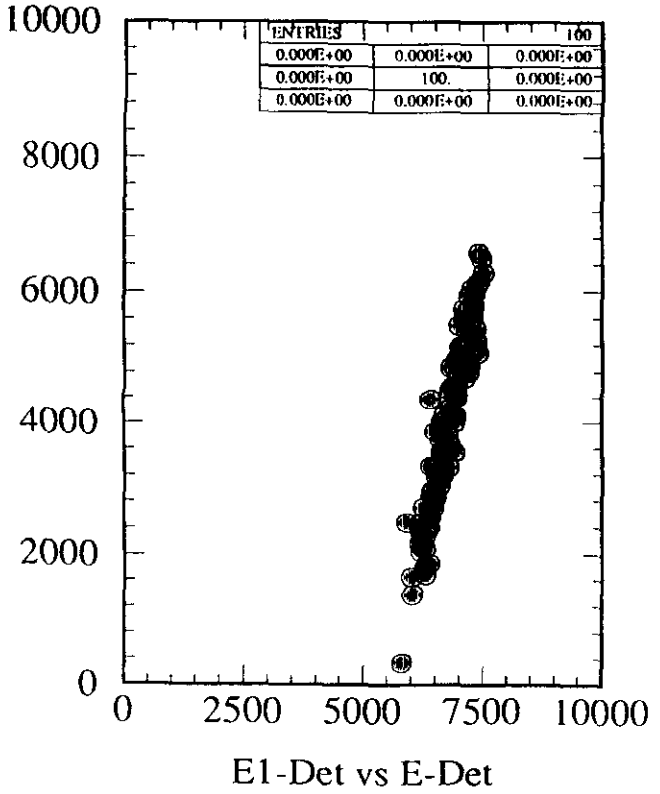
ENTRIES 100
0.000E+00 0.000E+00 0.000E+00
0.000E+00 100. 0.000E+00
0.000E+00 0.000E+00 0.000E+00
0 2000 4000 6000 8000 10000
0 2500 5000 7500 10000
E1-Det vs E-Det

Figure 11

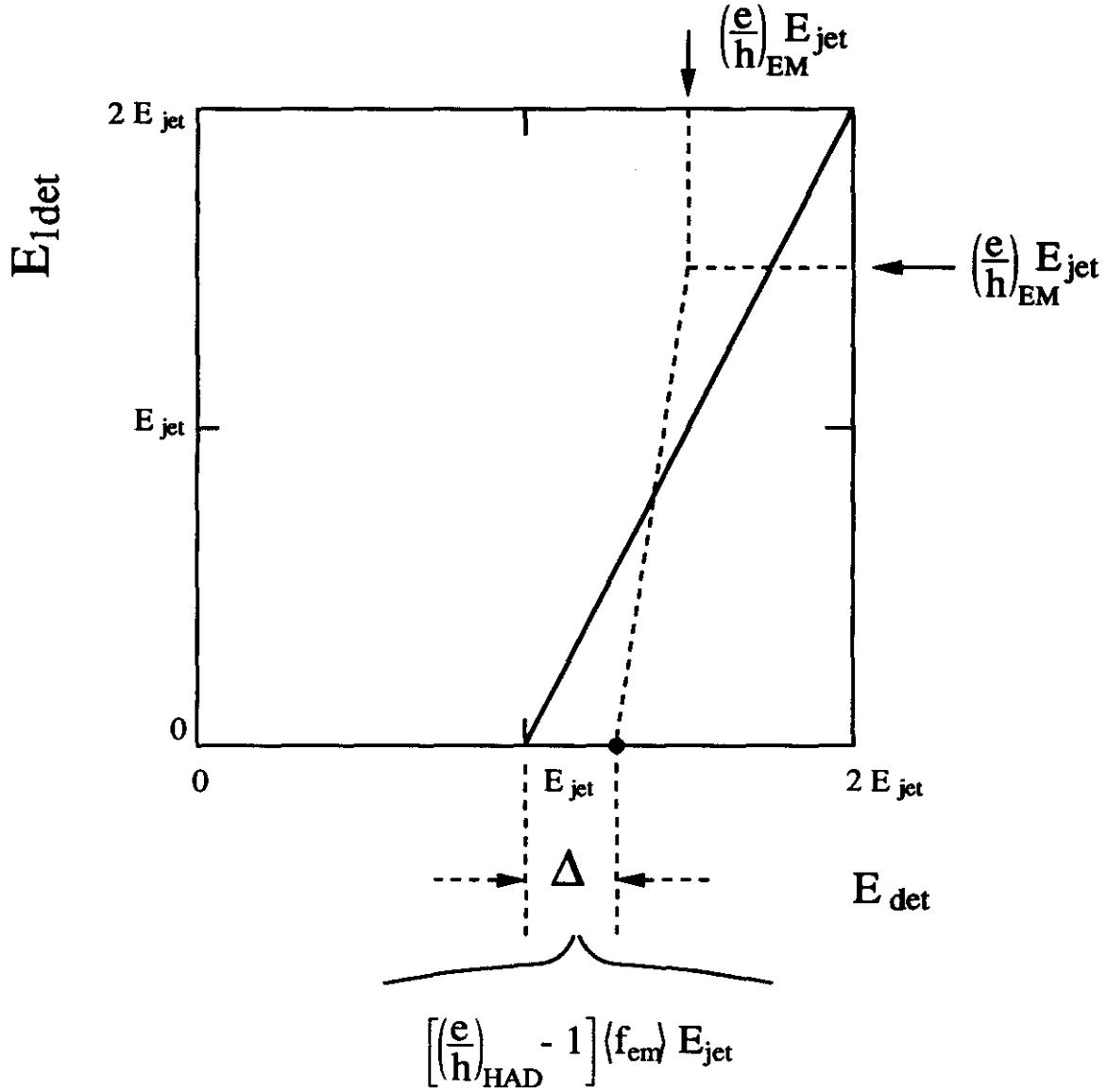
$\left(\frac{e}{h}\right)_{EM} E_{jet}$
$2\,E_{jet}$
E_{1det}
$\left(\frac{e}{h}\right)_{EM} E_{jet}$
E_{jet}
0
0
E_{jet}
$2\,E_{jet}$
Δ
E_{det}
$\left[\left(\frac{e}{h}\right)_{HAD} - 1\right]\langle f_{em}\rangle\, E_{jet}$

Figure 12